



The effect of the thermal heating on the magnetic properties of a high permeability amorphous $\text{Fe}_{76.5}\text{Cu}_1\text{Nb}_3\text{Si}_{13.5}\text{B}_6$ ribbon

E. B. Peixoto¹ · J. G. S. Duque¹ · L. S. Silva² · R. A. G. Silva³

Received: 1 February 2020 / Accepted: 23 February 2021 / Published online: 26 March 2021
© Akadémiai Kiadó, Budapest, Hungary 2021

Abstract

In this work, the effects of the thermal heating on an as-cast Fe-based amorphous ribbon treated in a conventional furnace are reported. We used thermogravimetry, differential scanning calorimetry, X-ray diffraction and M vs H measurements to characterize the samples. The transition temperatures of magnetic phases (amorphous residual matrix and Fe_3Si nanoparticles), which were estimated from thermogravimetric measurements, are thermal heat dependent. Besides, the analysis of the DSC data allows us to evaluate the crystallized fraction. From Rietveld refinement of the XRD diffraction patterns carried out after the DSC measurement, we confirm that the crystallized grains consist of Fe_3Si (suessite) nanocrystalline phase. The suessite phases should be embedded inside the residual amorphous matrix. Furthermore, we synthesized a Fe_3Si bulk sample using an arc furnace in order to compare its magnetic behavior with those Fe_3Si nanoparticles. Finally, the magnetic anisotropy also shows to be thermal heat dependent.

Introduction

It is well-known that, in amorphous materials, the long-range atomic order is not present. However, if these materials are formed by atoms with permanent magnetic moments, a long-range magnetic order can arise. A very important feature of amorphous magnetic materials is the possibility of manipulating their magnetic properties. Such manipulation can be achieved through the induction of specific anisotropies or heat treatments, either by conventional furnace or heating Joule [1–4]. The heating aims to reduce internal stresses induced during the growth process. In addition, in the case of Joule heating, the circular magnetic field generated by the passage of the current may promote the induction of a circular anisotropy. However, it is important to say that the heat treatment carried out through Joule heating is not homogeneous along the length of the sample [4]. From a point of view of technological applications, the soft

magnetic properties of amorphous metallic alloys have been the subject of intense studies during the last decades [5–9].

Among the wide varieties of amorphous alloys, the Fe-based amorphous compositions stand out [10–14], in which the soft magnetic properties are easily tunable. In particular, as we have said, the soft magnetic properties of amorphous alloys can be improved for submitting them to an annealing in conventional furnace or for using the joule heating [4, 11, 15]. Previous works argue that the outstanding soft magnetic properties in Fe-based amorphous compositions appear due the growth of noncrystalline grains, which are embedded inside the residual amorphous matrix [16–18]. The high magnetic permeability, which is usually found in these materials, can be related with the negligible magnetocrystalline anisotropy. Such interplay occurs due to the ultrafine structure, composed by ferromagnetic grains (average crystallites sizes 10 nm), embedded in the residual ferromagnetic amorphous phase. Noteworthy, most applications of such systems are based on their magnetic softness [19, 20], and thus it is very useful to determine the role of such fine particles in the high permeability behavior.

In this work, we study the magnetic properties as a function of crystallization of an amorphous magnetic $\text{Fe}_{76.5}\text{Cu}_1\text{Nb}_3\text{Si}_{13.5}\text{B}_6$ ribbon using thermal analysis, X-ray diffraction and magnetization measurements. Our data show that the Curie temperature increases as a function of the time of thermal heat. We argue that this fact can be associated

✉ J. G. S. Duque
gerivaldoduque@gmail.com

¹ Programa de Pós-Graduação em Física, Campus Prof. José Aluísio de Campos, UFS, São Cristóvão, SE 49100-000, Brazil

² Instituto Federal de Tocantins-IFTO-Campus Colinas do Tocantins, Colinas do Tocantins 77760-000, Brazil

³ Departamento de Química, UNIFESP, Diadema, SP, Brazil

with the growth of Fe_3Si phase inside residual amorphous matrix. Also, in this same sense, there is a change in magnetic anisotropy as a function of crystallized fraction of particles.

Experimental

A sample of the $\text{Fe}_{76.5}\text{Cu}_1\text{Nb}_3\text{Si}_{13.5}\text{B}_6$ amorphous ribbon (kindly supplied by Unitika Ltd) obtained by melt spinning was used in our experiments. Once Fe_3Si nanoparticles are grown during the recrystallization of the ribbons, for comparison, we also have obtained a Fe_3Si polycrystalline sample from stoichiometric amounts of the high purity iron and silicon elements melted in an arc furnace. After that, this pre-heated polycrystalline sample was annealed at 800°C in a conventional furnace for two weeks to ensure its homogenization [21]. Thermogravimetry data using a TGA Q50 TA Instruments were taken in the range $120 \leq T \leq 650^\circ\text{C}$. Besides the determination of the recrystallization temperatures, which is obtained using the temperature calibration procedure TG equipment, we were also able to estimate the Curie temperatures of the as-cast and annealed ribbons at $t_a = 540^\circ\text{C}$ for 1, 5, 10 and 20 minutes. In addition, differential scanning calorimetry (DSC) curves in isothermal and non-isothermal modes were obtained using a DSC Q20 TA Instruments. In this case, the non-isothermal measurements have been carried out in a wide range of temperature ($30 \leq T \leq 620^\circ\text{C}$). In order to avoid the oxidation process of samples, argon atmosphere with a flow of 50 mL min^{-1} was used in both isothermal and non-isothermal measures. The structural properties of the annealed ribbons were studied by X-ray diffraction (XRD) in a PANalytical Empyrean diffractometer using the Bragg-Brentano geometry in the angular range of $35 \leq \theta \leq 85^\circ$ with an angular step of 0.013° and a CuK_α radiation. The X-ray patterns were refined using the Rietveld method. Magnetization as a function of the magnetic field ($-60 \leq H \leq +60 \text{ kOe}$) was performed using a Lake Shore Cryogenics Vibrating Sample Magnetometer (VSM). It is important to note that once samples used in magnetization measurements have been heated in a conventional furnace, to avoid the oxidation, they were vacuum sealed in quartz tube.

Experimental results and discussion

Figure 1 shows the mass loss recorded in the temperature range from 120 to 650°C at $10^\circ\text{C min}^{-1}$ under an argon atmosphere for as-cast and heated ribbons at $t_a = 540^\circ\text{C}$ for 1, 5, 10 and 20 min. These measurements were performed following the calibration procedure described in Refs. [22–24]. It is important to note that the derivatives of

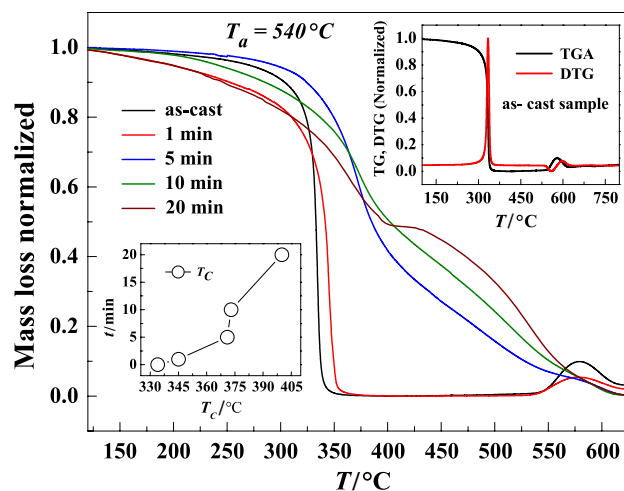


Fig. 1 (Color online) Mass loss data for the $\text{Fe}_{76.5}\text{Cu}_1\text{Nb}_3\text{Si}_{13.5}\text{B}_6$ ribbons: as-cast and heated at $t_a = 540^\circ\text{C}$ for 1, 5, 10 and 20 min. All measurements were done with heating rate of $10^\circ\text{C min}^{-1}$ (argon atmosphere) in the calibration mode of TGA. In the top inset, we show the TG and DTG for the as-cast sample. The bottom inset exhibits the T_C value of residual amorphous phase as a function of heating time

the TG curves (top inset) were taken in order to estimate the Curie temperatures, T_C (bottom inset), and the re-crystallization temperatures of as-cast and heated samples. It is evident that for the as-cast and heated samples with $t_a = 1$ min, the first ($T \approx 340^\circ\text{C}$) and second ($T \approx 540^\circ\text{C}$) abrupt mass losses should be associated with the magnetic transition temperature of the amorphous phase and the growth of the Fe_3Si nanoparticles, respectively. Noticeable, Lovas et al. [25] and Valenzuela et al. [10] have reported similar results of the Curie temperature of as-cast $\text{Fe}_{76.5}\text{Cu}_1\text{Nb}_3\text{Si}_{13.5}\text{B}_6$ ribbons using conventional magnetic techniques. For samples heated during 5, 10 and 20 min, the increase of the number of particles inside of residual amorphous matrix (described below in DSC analysis) changes the magnetic properties of samples. Besides, for all samples, the decreasing in the mass loss curve at $\approx 600^\circ\text{C}$ must be related with the Curie point of Fe_3Si phase. Finally, one must note that T_C of residual amorphous phase increases as a function of the annealing time. Interestingly, once the Fe_3Si phase is formed, there should be an increasing of mean Fe-Fe distance inside the residual amorphous phase, weakening the magnetic interaction strength. On the contrary, the experimental data show that the transition temperature of residual amorphous phase shifts to higher temperatures. Valenzuela et al. [10] and Ponpandian et al. [26] argue that this result can be related with the appearance of the cubic face centered phase $\alpha\text{-Fe}_3\text{Si}$ due to heat treatment.

Figure 2 presents the normalized DSC measurements for as-cast $\text{Fe}_{76.5}\text{Cu}_1\text{Nb}_3\text{Si}_{13.5}\text{B}_6$ ribbons at two different experimental conditions. Figure 2a shows the crystallized fraction

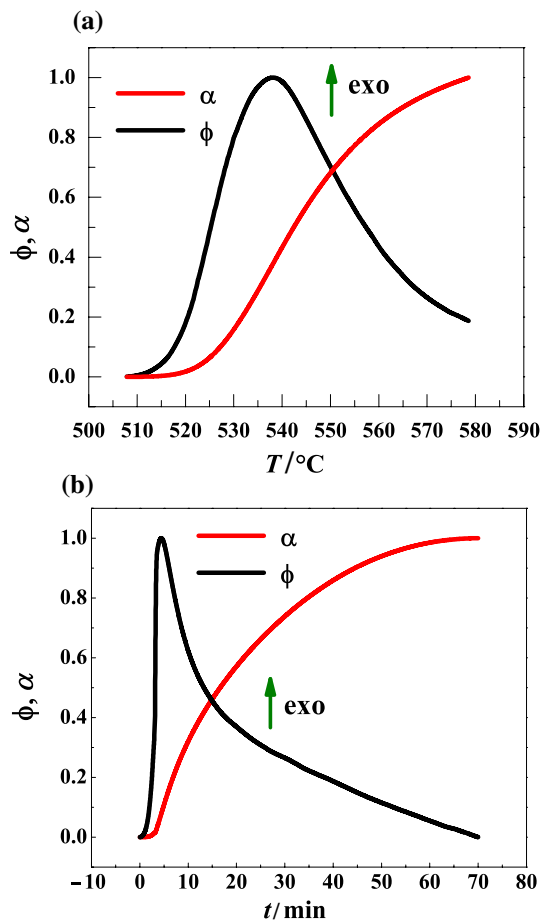


Fig. 2 (Color online) Normalized DSC curves for the as-cast $\text{Fe}_{76.5}\text{Cu}_1\text{Nb}_3\text{Si}_{13.5}\text{B}_6$ ribbons carried out to a heating rate of $15\text{ }^\circ\text{C min}^{-1}$ in argon atmosphere. **(a)** Non-isothermal curves and **(b)** isothermal (ϕ) curves and their respective crystallized fractions (α). The isothermal curves were taken at $T = 540\text{ }^\circ\text{C}$

and the correspondent heat flow for non-isothermal curves carried out with a rate of $15\text{ }^\circ\text{C min}^{-1}$ in the temperature range from 30 to $580\text{ }^\circ\text{C}$. Figure 2b shows the crystallized fraction and the isothermal measurement performed at $T = 540\text{ }^\circ\text{C}$. The crystallized fraction, α , was obtained through of the equation

$$\alpha = \frac{1}{\Delta H_C} \int_0^t \phi dt \tag{1}$$

where ΔH_C is the enthalpy of crystallization, which is calculated through the area of the heat flow, ϕ , curve as a function of time. The crystallized fraction shown in Fig. 2 is characteristic of the reaction profile sigmoid. The peak in DSC corresponds to an exothermic transformation confirming that the crystallization process is associated with grain growth.

Figure 3 displays the room temperature X-ray diffraction patterns for $\text{Fe}_{76.5}\text{Cu}_1\text{Nb}_3\text{Si}_{13.5}\text{B}_6$ amorphous ribbon after

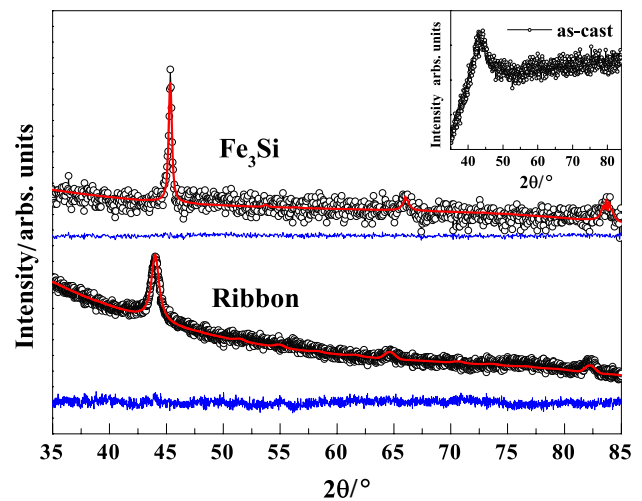


Fig. 3 (Color online) X-ray diffraction patterns using $\text{CuK}\alpha$ radiation for the $\text{Fe}_{76.5}\text{Cu}_1\text{Nb}_3\text{Si}_{13.5}\text{B}_6$ amorphous ribbon after TGA measurement. Moreover, for comparison, the XRD for Fe_3Si sample in bulk form is also shown

DSC measurement and Fe_3Si polycrystalline sample in its bulk form. The solid curves means the calculated pattern from the structural model used in the Rietveld refinement to fit the experimental data. The solid line in the bottom of the measurement is the difference between experimental and calculated data. In the inset, the XRD for the as-cast sample is presented. The broad peak $\approx 2\theta = 45^\circ$ is likely indicating that some degree of short-range atomic order is present. The analyzed XRD patterns are consistent with the *fcc* global symmetry, which crystallize in a DO_3 -type structure (ICSD 412838). Moreover, the analysis of the XRD pattern of heated ribbon sample allows us to estimate the mean sizes of the crystallized grains via Scherrer equation, which was approximately 13 nm.

Figure 4 shows magnetization as a function of the applied magnetic field (M vs H loops) at 300 K for the $\text{Fe}_{76.5}\text{Cu}_1\text{Nb}_3\text{Si}_{13.5}\text{B}_6$ ribbon heated for 2 min and the arc melting Fe_3Si sample. The magnetic field was applied parallel to the ribbon surface and, in the case of the bulk Fe_3Si , a thin rectangular sample was cut and the magnetic field was also applied parallel to its surface. It is worth to note that in both cases the saturation magnetization is $\approx 156\text{ emu g}^{-1}$, which is close to the bulk Fe_3Si sample [27]. This result reveals that despite the small heating time, the high field magnetization must be dominated by Fe_3Si nanoparticles for heated ribbon. Furthermore, M vs H loops do not present coercivity and remanence indicating the low anisotropy of both samples.

If one calculates the effective anisotropy, which must be proportional to the area between the M vs H and the M -axis [28], there is clearly an anisotropy enhancement. Once Fe_3Si nanoparticles embedded inside the residual matrix change

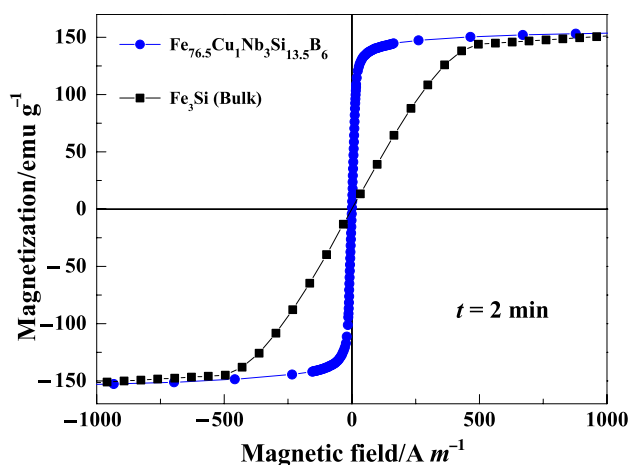


Fig. 4 (Color online) *MvsH* loops taken at $T = 300$ K for the Fe_3Si sample in its bulk form and $\text{Fe}_{76.5}\text{Cu}_1\text{Nb}_3\text{Si}_{13.5}\text{B}_6$ ribbon after a thermal heating at $T = 540$ °C for 2 min. In both cases, the magnetic field was applied parallel to the sample surface

with the thermal heat, crystallized fraction can play an important role in determining the magnetic anisotropy, that is, α is a determinant factor behind the magnetic softness of the ribbon.

In order to better visualize the change in the anisotropy likely produced by the thermal heating, which gives rise to a nanocrystals embedded inside a residual amorphous matrix, we show in Fig. 5a and b the *MvsH* curves for $\text{Fe}_{76.5}\text{Cu}_1\text{Nb}_3\text{Si}_{13.5}\text{B}_6$ ribbons annealed at 540 °C for 1 and 10 min as a function of the angle between the applied magnetic field and the sample surface. In Fig. 5c, we display the in-plane magnetization curves for the same ribbon heated at 540 °C for 1, 2, 4 and 10 min. The insets display the calculated magnetic anisotropy.

It is well known that the fabrication processes of the amorphous materials in the shape of wire, ribbons and glass-coated microwires can introduce peculiar distributions of magnetoelastic anisotropy [4]. However, previous works argue that the magnetoelastic anisotropy can be tuned through proper thermal treatments in conventional furnace or Joule heating [1, 2, 4, 29].

The crystallized fraction curves extracted from the isothermal measurement (see Fig. 2) allows us to state that the low-field magnetic response comes from only the amorphous matrix once the crystallized fraction is smaller than 5% to annealing times in the ranging $0 \leq t \leq 5$ min. However, the crystallized fraction can play an important role in the magnetic response at higher magnetic fields and/or to samples submitted to higher heating times. In the latter, the magnetic coupling between nanoparticles and the amorphous residual matrix can be determinant in the magnetic behavior.

The results shown in Fig. 5 are consistent with the change of the anisotropy (likely from magnetoelastic origin) of the

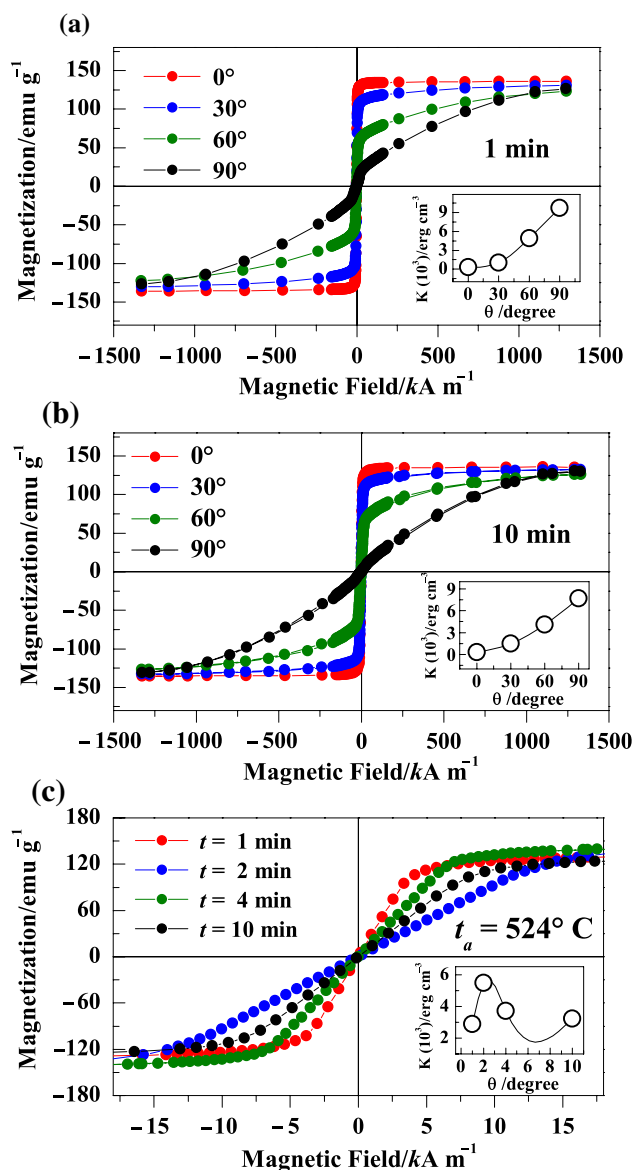


Fig. 5 (Color online) (a) and (b) *MvsH* loops as a function of the angle between the applied magnetic field and the $\text{Fe}_{76.5}\text{Cu}_1\text{Nb}_3\text{Si}_{13.5}\text{B}_6$ ribbon surface for a heating time of 1 and 10 min, respectively. **c** *MvsH* loops as a function of the heating time using for the previous field configuration. In the insets, we show the effective anisotropy calculated from the *MvsH* curves

heated ribbons. Moreover, in the case of angle-dependence, the change in the anisotropy can be associated to both magnetoelastic and shape anisotropies. Nevertheless, we note that the maximum values reached at $\theta = 90^\circ$ for samples heated for 1 and 10 min are 10 and 8 erg cm^{-3} , respectively. This difference can be attributed to the change in the magnetoelastic anisotropy contribution, which can be associated to nanocrystals grown inside the residual amorphous matrix. Furthermore, for the heating time-dependence of the anisotropy, it is possible to see that there is a maximum value at

an annealing time of 2 min. Indeed, previous works [16, 19] report that the magnetic softness appears after heating and can be interpreted as the dependence of the saturation magnetostriction with partial nanocrystallization of the ribbons.

Conclusions

In this work, thermal measurements TGA and DSC were used to study the crystallization processes of an amorphous $\text{Fe}_{76.5}\text{Cu}_1\text{Nb}_3\text{Si}_{13.5}\text{B}_6$ magnetic ribbon produced by the melt spinning technique and submitted to a thermal heating in a conventional furnace. The crystallization temperature was confirmed by means of an exothermic peak of DSC curve. Besides, a temperature calibration procedure of the thermogravimetric equipment allows us to determine the Curie temperature of both amorphous residual matrix and Fe_3Si magnetic phases. X-ray diffraction carried out for the heated sample shows the formation of nanocrystals of Fe_3Si with sizes of ≈ 13 nm. The M vs H loops performed for $\text{Fe}_{76.5}\text{Cu}_1\text{Nb}_3\text{Si}_{13.5}\text{B}_6$ ribbons annealed at 540 °C for 2 min and at different annealing times show a change in the effective magnetic anisotropy. This result seems to be dependent on the crystallized fraction of Fe_3Si nanocrystals, which is embedded inside residual amorphous matrix.

Acknowledgements We thank to the Brazilian agencies FAPITEC (PRONEX), CNPq (455608/2014-8 and 455970/2014-9), FAPESP (2015/18996-0) and the Coordenação de Aperfeiçoamento de Pessoal de Nível Superior - Brasil (CAPES) - Finance Code 001 for financial support.

References

- Kenny LA, José MM, Mihail I, Lourdes D, Julian G. Magnetic properties of annealed amorphous $\text{Fe}_{72.5}\text{Si}_{12.5}\text{B}_{15}$ alloy obtained by gas atomization technique. *IEEE Trans Magn.* 2018;54(11):2002405. <https://doi.org/10.1109/TMAG.2018.2839258>.
- Cao CC, Wang YG, Zhu L, Meng Y, Dai YD, Chen JK. Evolution of structural and magnetic properties of the FeCuBP amorphous alloy during annealing. *J Alloy Compd.* 2017;722:394. <https://doi.org/10.1016/j.jallcom.2017.06.147>.
- González J, Murillo N, Blanco JM, González JM, and Kulik T. Stress annealing in $\text{Fe}_{73.5}\text{Cu}_1\text{Ta}_3\text{Si}_{13.5}\text{B}_9$ amorphous alloy: Induced magnetic anisotropy and variation of the magnetostriction constant. *J Appl Phys* 1994; 76:1131. <https://doi.org/10.1063/1.357834>.
- Knobel M, Allia P, Gomez-Polo C, Chiriac H, Vazquez M. Joule heating in amorphous metallic wires. *J Phys D Appl Phys.* 1995;28:2398. <https://doi.org/10.1088/0022-3727/28/12/002>.
- Pang LL, Inoue A, Zanaeva EN, Wang F, Bazlov AI, Han Y, Kong FL, Zhu SL, Shull RB. Nanocrystallization, good soft magnetic properties and ultrahigh mechanical strength for $\text{Fe}_{82-85}\text{B}_{13-16}\text{Si}_1\text{Cu}_1$ amorphous alloys. *J Alloy Compd.* 2019;785:25. <https://doi.org/10.1016/j.jallcom.2019.01.150>.
- Sicheng Z, Zhenrui P, Yafeng G, Zhe D, Wen W, Yan W. Soft magnetic properties and corrosion resistance of Fe-Co-B-M ($M = \text{Nb, Ta}$ and NbNi) metallic glasses. *J Non-Cryst Solids.* 2019;506:28. <https://doi.org/10.1016/j.jnoncrysol.2018.11.029>.
- Xingdu F, Tao Z, Mufeng J, Weiming Y, Baolong S. Synthesis of novel FeSiBPCCu alloys with high amorphous forming ability and good soft magnetic properties. *J Non-Cryst Solids.* 2019;503–504:36. <https://doi.org/10.1016/j.jnoncrysol.2018.09.021>.
- Jaafari Z, Seifoddini A, Hasani S, Rezaei-Shahreza P. Kinetic analysis of crystallization process in $[(\text{Fe}_{0.9}\text{Ni}_{0.1})_{77}\text{Mo}_5\text{P}_9\text{C}_{7.5}\text{B}_{1.5}]_{100-x}\text{Cu}_x$ ($x = 0.1$ at.%) BMG. *J Therm Anal Calorim.* 2018;134:1565. <https://doi.org/10.1007/s10973-018-7372-y>.
- Ouyang S, Song LJ, Liu YH, Huo JT, Wang JQ, Xu W, Li JL, Wang CT, Wang XM, Li RW. Correlation between the viscoelastic heterogeneity and the domain wall motion of Fe-based metallic glass. *Phys Rev Mater.* 2018;2:063601. <https://doi.org/10.1103/PhysRevMaterials.2.063601>.
- Valenzuela LA, Duque JGS, Meneses CT, Nunes WC, Knobel M. Structural and magnetic properties of nanocrystalline particles in an amorphous $\text{Fe}_{73.5}\text{Nb}_3\text{CuSi}_{13.5}\text{B}_9$ matrix. *J Non-Cryst Solids.* 2008;354:4871. <https://doi.org/10.1016/j.jnoncrysol.2008.04.039>.
- Yu-rong J, Zhi W, Fang W, Ye H, Zhong-yan X, Li-juan L, Li Z. Effect of P substitution for Nb on structure and soft magnetic properties of Si-rich FeCuNbSiB nanocrystalline alloys. *Mater Sci Eng B.* 2017;222:55. <https://doi.org/10.1016/j.mseb.2017.04.007>.
- Shalygina EE, Bekoeva LM, Shalygin AN. Properties of micro-magnetic structures in amorphous FeCuNbSiB alloys. *Tech Phys Lett.* 1999;25(1):26. <https://doi.org/10.1134/1.1262369>.
- Hono K, Ping DH, Ohnuma M, Onodera H. Cu clustering and Si partitioning in the early crystallization stage of an $\text{Fe}_{73.5}\text{Si}_{13.5}\text{B}_9\text{Nb}_3\text{Cu}_1$ amorphous alloy. *Acta Mater.* 1999;47(3):997. [https://doi.org/10.1016/s1359-6454\(98\)00392-9](https://doi.org/10.1016/s1359-6454(98)00392-9).
- Takenaka K, Setyawan AD, Sharma P, Nishiyama N, Makino A. Industrialization of nanocrystalline Fe-Si-B-P-Cu alloys for high magnetic flux density cores. *J Magn Magn Mater.* 2016;401:479. <https://doi.org/10.1016/j.jmmm.2015.10.091>.
- Pradeep KG, Herzer G, Choi P, Raabe D. Atom probe tomography study of ultrahigh nanocrystallization rates in FeSiNbBCu soft magnetic amorphous alloys on rapid annealing. *Acta Mater.* 2014;68:295. <https://doi.org/10.1016/j.actamat.2014.01.031>.
- Herzer G. Grain size dependence of coercivity and permeability in nanocrystalline ferromagnets. *IEEE Trans Magn.* 1990;26(5):1397. <https://doi.org/10.1109/20.104389>.
- Herzer G. Anisotropies in soft magnetic nanocrystalline alloys. *J Magn Magn Mater.* 2005;294:99. <https://doi.org/10.1016/j.jmmm.2005.03.020>.
- Suzuki K, Herzer G, Cadogan JM. The effect of coherent uniaxial anisotropies on the grain-size dependence of coercivity in nanocrystalline soft magnetic alloys. *J Magn Magn Mater.* 1998;177–181:949. [https://doi.org/10.1016/S0304-8853\(97\)00987-6](https://doi.org/10.1016/S0304-8853(97)00987-6).
- Herzer G. Soft magnetic nanocrystalline materials. *Scr Metall Mater.* 1995;33(10/11):1741. [https://doi.org/10.1016/0956-716X\(95\)00397-E](https://doi.org/10.1016/0956-716X(95)00397-E).
- Herzer G, Budinsky V, Polak C. Magnetic properties of nanocrystalline FeCuNbSiB with huge creep induced anisotropy. *J Phys Conf Ser.* 2011;266:012010. <https://doi.org/10.1088/1742-6596/266/1/012010>.
- Lataifeh MS, O'Shea M, Saleh AS, Mahmood SH. Magnetization Measurements on gas Prepared Aslshhca and Annealed $\text{Fe}_{3-x}\text{Mn}_x\text{Si}$ Alloys. *Jordan J Phys.* 2008;1(1):31.
- Gallagher PK, Gyorgy EM. Curie temperature standards for thermogravimetry: the effect of magnetic field strength and comparison with melting point standards using Ni and Pb. *Thermochim Acta.* 1986;109:193. [https://doi.org/10.1016/0040-6031\(86\)85021-3](https://doi.org/10.1016/0040-6031(86)85021-3).

23. Legendre B, Sghaier M. Curie temperature of nickel. *J Therm Anal Calorim.* 2011;105:141. <https://doi.org/10.1007/s10973-011-1448-2>.
24. Peixoto EB, Mendonça EC, Mercena SG, Jesus ACB, Barbosa CCS, Meneses CT, Duque JGS, Silva RAG. Study of the dynamic of crystallization of an amorphous $\text{Fe}_{40}\text{Ni}_{40}\text{P}_{14}\text{B}_6$ ribbon through Johnson-Mehl-Avrami model. *J Alloy Compd.* 2018;731:1275. <https://doi.org/10.1016/j.jallcom.2017.10.062>.
25. Lovas A, Kiss LF, Balogh I. Saturation magnetization and amorphous Curie point changes during the early stage of amorphous nanocrystalline transformation of a FINEMET-type alloy. *J Magn Magn Mater.* 2000;215–216:463. [https://doi.org/10.1016/S0304-8853\(00\)00189-X](https://doi.org/10.1016/S0304-8853(00)00189-X).
26. Ponpandian N, Narayanasamy A, Chattopadhyay K, Manivel Raja M, Ganesan K, Chinnasamy CN, Jeyadevan B. Low-temperature magnetic properties and the crystallization behavior of FINEMET alloy. *J Appl Phys.* 2003;93(10):6182. <https://doi.org/10.1063/1.1565829>.
27. Hines WA, Menotti AH, Budnick JI, Burch TJ, Litrenta T, Niculescu V, Raj K. *Phys Rev B.* 1976;13:4060. <https://doi.org/10.1103/PhysRevB.13.4060>.
28. Cullity B.D. *Introduction to Magnetism and Magnetic Materials.* 1 ed. Addison-Wesley Publishing Company; 1972. pp. 207–246.
29. Kim CG, Kim JB, Yoon SS, Jang KJ, Kim CO. Temperature dependence of asymmetric GMI profile. *J Magn Magn Mater.* 2001;226–230:700. [https://doi.org/10.1016/S0304-8853\(00\)01141-0](https://doi.org/10.1016/S0304-8853(00)01141-0).

Publisher's Note Springer Nature remains neutral with regard to jurisdictional claims in published maps and institutional affiliations.